

Structural Modulation of Chromic Response: Effects of Binding-Site Blocking in a Conjugated Calix[4]pyrrole Chromophore

Václav Březina,^[a, b] Shinsuke Ishihara,^[a] Jan Lang,^[b] Lenka Hanyková,^[b] Katsuhiko Ariga,^[a, c] Jonathan P. Hill,^{*[a]} and Jan Labuta^{*[a, d]}

Herein, we modulate the chromic response of a highly colored tetrapyrrole macrocycle, namely, tetrakis(3,5-di-*tert*-butyl-4-oxocyclohexadien-2,5-yl)porphyrinogen (OxP) by structural modification. N-Benzylation at the macrocyclic nitrogen atoms leads to stepwise elimination of the two calix[4]pyrrole-type binding sites of OxP and serial variation of the chromic properties of the products, double N-benzylated Bz₂OxP and tetra N-benzylated Bz₄OxP. The halochromic (response to acidity) and solvatochromic (response to solvent polarity) properties were studied by using UV/Vis spectroscopy and NMR spectroscopy in

nonpolar organic solvents. Titration experiments were used to generate binding isotherms to elucidate their binding properties with difluoroacetic acid. Differences in the halochromic properties of the compounds allowed construction of a colorimetric scale of acidity in nonpolar solvents, as the compounds in the series OxP, Bz₂OxP, and Bz₄OxP are increasingly difficult to protonate but maintain their propensity to change color upon protonation. The concurrent effects of binding-site blocking and modulation of acidity sensitivity are important new aspects for the development of colorimetric indicators.

1. Introduction

Variation in the color of a dye or pigment due to changes in its immediate environment is referred to as chromism. It is a key feature that has led to sensing applications, perhaps most importantly involving acid–base equilibria^[1,2] (e.g. halochromism of pH indicators). It has also been exploited in the delineation of solvent polarity (i.e. solvatochromism) and for the construction of polarity scales such as the E_T(30)^[3] and Z scales.^[4,5]

Several other chromic phenomena exist for which organic pigment molecules change color in response to an applied stimulus, including light,^[6] pressure,^[7] and temperature.^[8] Chromic events are typically reversible adding to their attractiveness for various applications. For example, acid–base reactions can be monitored according to reversible color changes that occur during forward and backward titration procedures of usually colorless analytes. Classically, many analytical procedures that rely on halochromism have been performed in aqueous solutions, although there are several reported methods applicable in nonpolar solvents^[9–11] sometimes involving visualization of an acid–base reaction by using a dye of appropriate structure.

The term halochromism (sometimes acidochromism), originally coined by Baeyer^[12] and recently resurrected by Reichardt,^[13] describes color changes that some dyes undergo in response to interactions with acid, base, or salt ions. Halochromic molecules (e.g. phenolphthalein, a component of Universal Indicator)^[14] interact with ions or are protonated (deprotonated) by acids (bases), which is usually accompanied by the appearance of new electronic absorption bands caused by variation in the conjugated structure of the halochromic dye. Color variation results from the different relative fractions of the halochromic dye in its different states of electronic conjugation. In contrast, solvatochromism occurs if the electronic ground and excited states of a chromophore are stabilized to different extents by solvents of differing polarities. This affects the energy difference between the ground and excited states, which results in shifts in the electronic absorption maxima (hypso- or bathochromic shift). A typical solvatochromic substance is Reichardt's dye,^[13] the behavior of which is the basis for the E_T(30) polarity scale. Despite its impressive solvatochromic

[a] V. Březina, Dr. S. Ishihara, Prof. K. Ariga, Dr. J. P. Hill, Dr. J. Labuta
International Center for Materials Nanoarchitectonics (WPI-MANA)
National Institute for Materials Science (NIMS)
1-1 Namiki, Tsukuba, Ibaraki 305-0044 (Japan)
E-mail: Jonathan.Hill@nims.go.jp
Labuta.Jan@nims.go.jp

[b] V. Březina, Dr. J. Lang, Dr. L. Hanyková
Faculty of Mathematics and Physics, Charles University
V Holešovičkách 2, 180 00 Prague 8 (Czech Republic)

[c] Prof. K. Ariga
Department of Advanced Materials Science
Graduate School of Frontier Sciences, The University of Tokyo
5-1-5 Kashiwanoha, Kashiwa, Chiba 277-8561 (Japan)

[d] Dr. J. Labuta
International Center for Young Scientists (ICYS-SENGEN)
National Institute for Materials Science (NIMS)
1-2-1 Sengen, Tsukuba, Ibaraki 305-0047 (Japan)

Supporting Information and the ORCID identification number(s) for the author(s) of this article can be found under <https://doi.org/10.1002/open.201800005>.

© 2018 The Authors. Published by Wiley-VCH Verlag GmbH & Co. KGaA. This is an open access article under the terms of the Creative Commons Attribution-NonCommercial-NoDerivs License, which permits use and distribution in any medium, provided the original work is properly cited, the use is non-commercial and no modifications or adaptations are made.

mic properties, Reichardt's dye loses its solvatochromism upon protonation, albeit reversibly.^[13,15]

Tetrapyrrole macrocycles compose a widely studied class of organic molecules that includes the porphyrins and other highly colored pigments known for their incorporation into biological photosynthetic and catalytic systems.^[16] Free-base porphyrins (i.e. those not containing a central chelated metal cation) are known to exhibit chromic properties, including halochromism, due to protonation at the central imino nitrogen atoms,^[17–19] and aggregachromism^[20,21] (due to excitonic coupling interactions in stacked aggregates). Although typical free-base porphyrins (e.g. *meso*-tetraphenylporphyrin) exhibit strong coloration and their electronic structures have been intensively investigated,^[22] it is perhaps surprising that they have not been studied in depth for their solvatochromic properties. This is because, notwithstanding their chromism in acidic media (halochromism), they tend to exhibit only small hypso- and bathochromic shifts in their absorption maxima in different solvents, leading to only weak variation in hue.^[23] Metalloporphyrins can exhibit stronger solvatochromism due to interactions between chelated metal cations and a polar coordinating solvent.^[24,25] Furthermore, structural changes (e.g. N-confusion)^[26,27] have been found to lead to significant solvatochromism, whereas the inherent synthetic flexibility of porphyrins can be used to design more complicated solvatochromic systems.^[28] Thus, although free-base porphyrins themselves have limited appeal as solvatochromic dyes, there are several classes of more complex derivatives, including N-confused porphyrins, that fulfil the requirements of strong color variation simply on the basis of solvent polarity.

In previous work,^[9] we used an oxoporphyrinogen dye (i.e. **OxP**, a conjugated calix[4]pyrrole,^[29–33] Figure 1 a) to monitor acid–base reactions in nonpolar solvents and found that it could be incorporated into dye films for application as an acidity indicator by similar means to those applied for Universal Indicator. The **OxP** molecular structure can be variously modified by alkylation at its macrocycle core nitrogen atoms (Figure 1),^[34–36] and we were intrigued to assess the influence of N-alkylation on the chromic properties of the **OxP** chromophore, in particular, in relation to a perceived reduction in flexibility of the macrocycle caused by steric crowding at its core. We chose the simple N_{21},N_{23} -bis(4-bromobenzyl) (**Bz₂OxP**, Figure 1 b) and $N_{21},N_{22},N_{23},N_{24}$ -tetrakis(4-bromobenzyl) (**Bz₄OxP**, Figure 1 c) derivatives of **OxP** (4-bromobenzyl derivatives are more soluble than the corresponding non-brominated derivatives). Differences in their substitution-dependent geometries as obtained from X-ray crystallography are shown in Figure 1.

Herein, we study protonation and the related chromic behavior (i.e. halochromism) of these **OxP** derivatives in nonpolar solvent/acid mixtures. We show that N-alkylation of **OxP** at its core nitrogen atoms substantially modulates chromic sensitivity to acid content over a broad range of volume fractions (vol.f. or φ) from 10^{-7} (in the case of **OxP**) to nearly 1 (for **Bz₄OxP**). We also investigate the solvatochromic properties of **OxP** derivatives in polar/nonpolar solvent mixtures in the absence of acid. Halo- and solvatochromic effects are rationalized

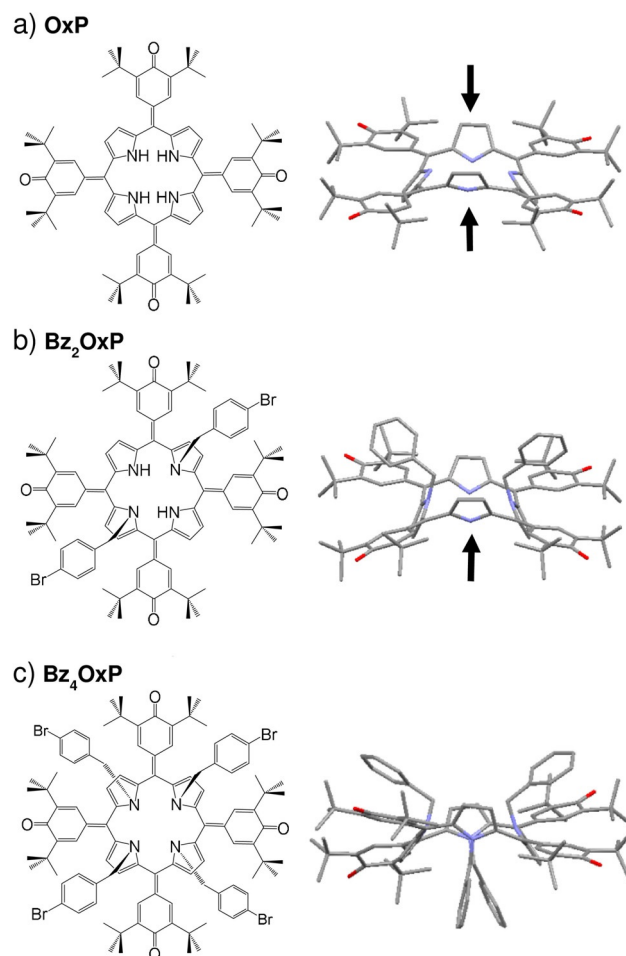


Figure 1. Chemical structures (left) and X-ray crystal structures (right) of a) oxoporphyrinogen (**OxP**), b) bis(4-bromobenzyl)oxoporphyrinogen (**Bz₂OxP**), c) tetrakis(4-bromobenzyl)oxoporphyrinogen (**Bz₄OxP**) used in this work. Dihedral angles between opposing pyrrole groups are shown. X-ray crystal structure in panels b, c are of the non-brominated derivatives.^[37] Accessible calix[4]pyrrole-type binding sites are denoted by arrows.

in terms of stepwise protonations and solvating interactions, respectively.

2. Results and Discussion

2.1. Halochromism of OxP

Previously, we reported the colorimetric response of **OxP** to trifluoroacetic acid (TFA),^[9] for which color variation upon the addition of acid was caused by the presence of di- and tetraprotonated species. In that case, fourfold protonation at the hemiquinonoid carbonyl sites was proven by direct observation of the intensity of the C–O–H infrared vibration. Here, we reanalyzed the UV/Vis data from that study from the point of view of its halochromic and solvatochromic properties. Spectra and analyses are shown in Figure 2. Singular value decomposition^[38–41] (SVD) of the spectra indicates the presence of three absorbing species (Figure S1 in the Supporting Information, for details about the implementation of SVD, see the Supporting

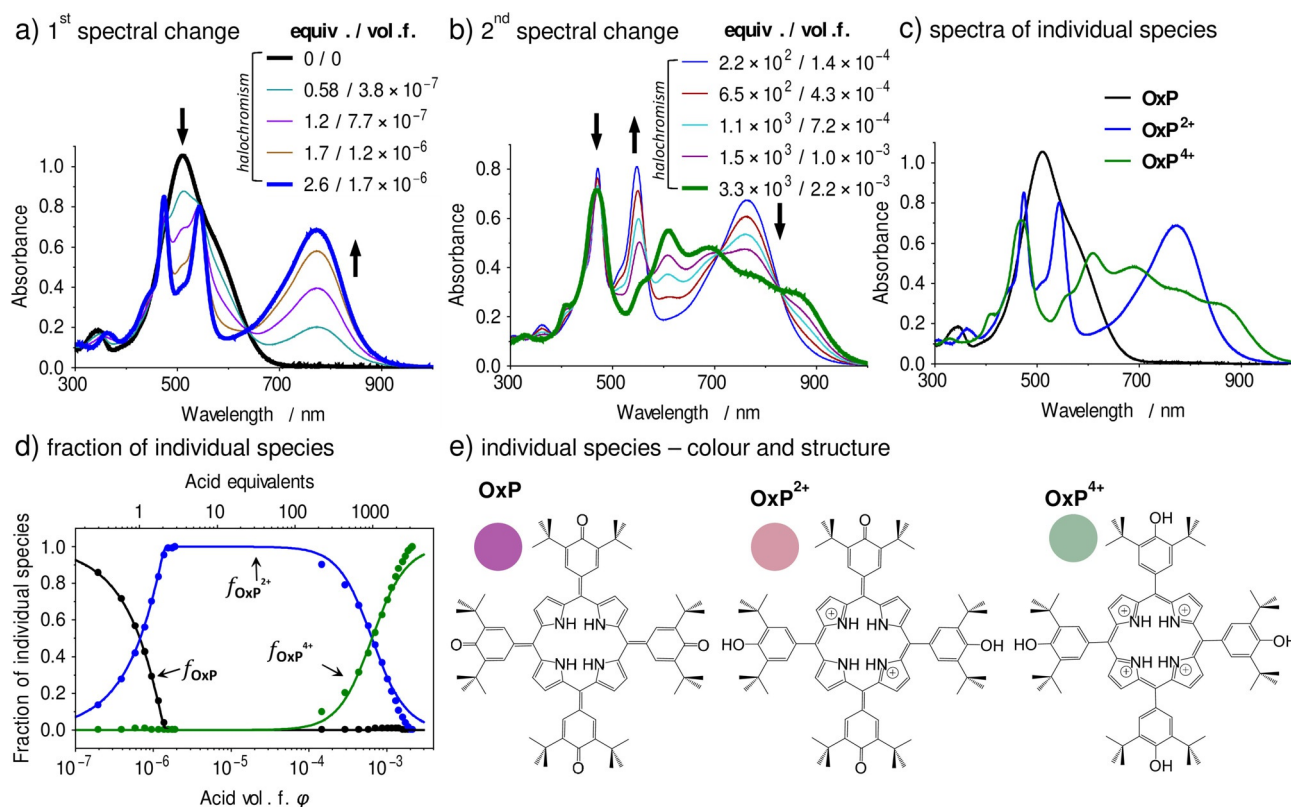


Figure 2. UV/Vis titration of **OxP** (10^{-5} M in CH_2Cl_2) with TFA on the basis of the data of Shundo et al.^[9] a,b) First and second sets of spectral changes occurring during titration. c) Spectra of individual absorbing species identified as the start and endpoints of each spectral change (bold lines in panels a, b). d) Relative fractions of absorbing species obtained from SVD by fitting to a 1:4 binding model (solid line); coefficients obtained by DSIS decomposition (solid circles). The same data in linear scale can be seen in Figure S14 a. e) Chemical structures and RGB colors of absorbing species (colors calculated from the spectra shown in panel c). The RGB coordinates are: **OxP** (R = 177, G = 92, B = 170), **OxP²⁺** (R = 212, G = 152, B = 166), and **OxP⁴⁺** (R = 151, G = 186, B = 160). Assignment of the chemical structures (including tautomeric processes) is given in Figure 11.

Information), which is confirmed by the presence of isobestic points in both consecutive sets of spectral changes (Figure 2a,b). The spectra of di- and tetraprotonated species (Figure 2c) were obtained, respectively, as the endpoints of each set of spectral changes (Figure 2a,b). We find that all experimentally observed UV/Vis spectra $S_{\text{obs}}(\varphi)$ are essentially simple linear combinations of spectra of the three individual absorbing species, **OxP**, **OxP²⁺**, and **OxP⁴⁺**, with acid volume fraction (φ) dependent coefficients, which can be expressed by the following equation [Eq. (1)]:

$$S_{\text{obs}}(\varphi) = f_{\text{OxP}}(\varphi) \times S_{\text{OxP}} + f_{\text{OxP}^{2+}}(\varphi) \times S_{\text{OxP}^{2+}} + f_{\text{OxP}^{4+}}(\varphi) \times S_{\text{OxP}^{4+}} \quad (1)$$

in which S_{OxP} , $S_{\text{OxP}^{2+}}$, and $S_{\text{OxP}^{4+}}$ are the spectra of the individual species **OxP**, **OxP²⁺**, and **OxP⁴⁺**, respectively, and $f_{\text{OxP}}(\varphi)$, $f_{\text{OxP}^{2+}}(\varphi)$, and $f_{\text{OxP}^{4+}}(\varphi)$ are the relative molar fractions of the corresponding individual species with constraints of non-negativity and obeying the unity condition, $f_{\text{OxP}}(\varphi) + f_{\text{OxP}^{2+}}(\varphi) + f_{\text{OxP}^{4+}}(\varphi) = 1$. We refer to this spectral separation process as “decomposition into the spectra of individual species” (DSIS). The result of DSIS is shown in Figure 2d (solid circles), for which the $f_{\bullet}(\varphi)$ (subscript “ \bullet ” denotes any individual species) values

are plotted as a function of φ . The quality of DSIS is excellent, as seen in Figure S2. In the presence of a solvatochromic shift, decomposition on the basis of Equation (1) is not possible (e.g. for spectra of Reichardt’s dye, see Figures S12 and S13). Therefore, there is no observable solvatochromic shift for **OxP** under these conditions, and color variation is caused by the presence of a few different conjugated species having different UV/Vis spectra. Thus, variation of the acid volume fraction φ affects the relative fraction of individual absorbing species but does not influence excitation energy levels, and **OxP** exhibits typical halochromism in TFA/ CH_2Cl_2 solvent mixtures.

Subsequently, we attempted to describe the interaction of **OxP** with TFA in terms of a host–guest binding model (in the frame of SVD, see Section S2 in the Supporting Information). Saturation of the **OxP** color changes is reached at low concentrations of TFA (0.002 vol.f. in CH_2Cl_2) so that equations governing the chemical equilibria can be used without corrections for activity. A 1:4 **OxP**:TFA stoichiometry binding model (for details about derivation of the binding isotherms see Section S1 in the Supporting Information) was adopted to obtain the equilibrium binding constants listed in Table 1. The resulting dependence (on φ) of the relative fractions of individual species is shown in Figure 2d (solid lines). The very good match of the fit can be seen in Figures S1d and S2. The dipro-

Table 1. Stepwise binding constants^[a] (decadic logarithm of numeric values of K_n are shown; all K_n have unit m^{-1}) and corresponding cooperativities^[b] determined by fitting of the NMR and UV/Vis titration experiments.

	DFA/TFA	UV/Vis	Camphorsulfonic acid	
	OxP		NMR	UV/Vis
$\log K_1$	4.5–8.7 ^[c]	2.3–6.0 ^[d]	4.0–5.0	N/A
$\log K_1K_2$	8.0–16 ^[c]	13–15 ^[d]	10–12	N/A
$\log K_3$	2.5–4.0 ^[c]	< 1.0 ^[d]	< 5.0	N/A
$\log K_3K_4$	4.0–6.0 ^[c]	3.6–5.0 ^[d]	2.3–2.5	N/A
$\log \alpha_{12}$	—	6.2 ^[d]	—	N/A
$\log \alpha_{34}$	—	> 2.2 ^[d]	—	N/A
Bz₂OxP				
$\log K_1$	3.0–3.2 ^[c]	3.2–3.3 ^[c]	4.5–5.1	4.6–4.8
Bz₄OxP				
$\log K_1$	–0.3–1.5 ^[c]	N/A	no change	no change

[a] Binding constants for processes at higher acid vol.f. could not be obtained because of the solubility threshold of camphorsulfonic acid and the unknown activity coefficients of the species in solution. Due to the nature of the binding processes and the models used, only the range of the binding constants could be determined. Also, due to the high cooperativity, overall binding constants (i.e. K_1K_2 , K_3K_4) were used instead of stepwise. Details about the binding models used are shown in the Supporting Information. [b] Cooperativity $\alpha_{12} = 4K_2/K_1$ was determined at the geometric mean of the minimum and maximum possible values of the binding constant, K_1 . Cooperativity α_{34} could only be restricted by using the formula $\alpha_{34} > 4(K_3K_4)_{\min}/K_{3\max}^2$ (where subscripts min and max indicate minimum value of K_3K_4 product and maximum value of K_3 , respectively), as there was no lower boundary for K_3 . Only UV/Vis measurements were used due to higher accuracy. [c] Measured with DFA. [d] Measured with TFA.

tonated form is stabilized by binding of two counteranions (on the top and on the bottom) at the central NH groups and by a tautomeric process.^[42] The excellent quality of the data fit also indicates the low stability of any mono- and triprotonated OxP species, which are essentially absent due to the ease of further protonation (analogous with tetraphenylporphyrin monocation^[43–45]). On the basis of this analysis the chemical structures including the changes in conjugation of the individual species are given in Figure 2 e.

2.2. Halochromism of Bz₂OxP

Bz₂OxP differs from OxP in that only single counteranion stabilization is allowed due to its double N-alkylation and consequent effective blocking of one of the two binding sites (Figure 1 b). For this reason, a stable monoprotinated Bz₂OxP⁺ form is readily formed. UV/Vis titration experiments of Bz₂OxP with difluoroacetic acid (DFA), which was used because of its nonexchanging hydrogen utilized in NMR spectroscopy analysis, reveal three consecutive spectral changes (Figure 3 a–c) and consequently four individual species (confirmed by SVD, see Figure S3). These have clear pseudosaturation points so that the spectra of the individual protonated species can be easily extracted at the respective endpoints (Figure 3 d). Assignment of the two- and fourfold protonation products as in-

dividual spectra is based on their significant similarities to S_{OxP2+} and S_{OxP4+} (see Figure 4 c,d). Assignment of the UV/Vis spectrum due to Bz₂OxP⁺ is supported by fitting of its binding constant (Table 1) and by NMR spectroscopy analysis (see Figure 5 and Figures S17 and S18). Similar to the OxP case, the linear combination of these four absorption spectra of the individual species accounts for all other experimentally observed spectra. This can be expressed in the following equation in which the terms have analogous meanings as in Equation (1) [Eq. (2)]:

$$S_{\text{obs}}(\varphi) = f_{\text{Bz}_2\text{OxP}}(\varphi) \times S_{\text{Bz}_2\text{OxP}} + f_{\text{Bz}_2\text{OxP}^+}(\varphi) \times S_{\text{Bz}_2\text{OxP}^+} + f_{\text{Bz}_2\text{OxP}^{2+}}(\varphi) \times S_{\text{Bz}_2\text{OxP}^{2+}} + f_{\text{Bz}_2\text{OxP}^{4+}}(\varphi) \times S_{\text{Bz}_2\text{OxP}^{4+}} \quad (2)$$

The results of DSIS decomposition are shown in Figure 3 e (solid circles), in which $f_{\bullet}(\varphi)$ (subscript “•” denotes any individual species) values are plotted as a function of φ . The excellent match of DSIS (Figure S4) confirms that Bz₂OxP is also a halochromic dye.

We again attempted to describe the interactions of Bz₂OxP with DFA in terms of a host–guest binding model. The first spectral change (up to vol.f. $\varphi = 0.001$ of DFA) was fitted by using a 1:1 Bz₂OxP:DFA binding model (Figure 3 e, solid lines), see Table 1. Details of the fitting procedure can be found in Figures S3 d and S4. Quantities of acid greater than vol.f. $\varphi = 0.001$ change the polarity of the solvent so that activity coefficients cannot be approximated as concentrations. Consequently, a simple binding model is not applicable for higher protonated states of Bz₂OxP beyond monoprotonation. NMR spectroscopy confirms protonation at the carbonyl oxygen atoms of the hemiquinonoid groups, and this leads to their increasing hydroxyphenyl character. This enables rotation of these groups about their *meso*-position bonds due to increased single-bond character, as can be seen in Figure 5. In addition, the phenolic type OH group around $\delta = 6.4$ ppm can also be observed in Figures S17, S18, and S22 b. The chemical identities of the individual species and their respective colors are given in Figure 3 f.

2.3. Chromism of Bz₄OxP

Of the compounds studied, Bz₄OxP is the least susceptible to protonation due to complete N-alkylation and consequent blockage of both central binding sites so that no potentially stabilizing ion-pair interactions with counteranions are allowed. UV/Vis titration with DFA (Figure 6 a,b) shows three sets of spectral changes. The first one (up to $\varphi = 0.01$) is a slight bathochromic shift due to hydrogen bonding of acid molecules to the carbonyl oxygen atoms (Figure 6 a, green arrow) without significant variation in the shape of the spectrum, which was not observed in the previous cases. This effect is attributed to solvatochromism. The corresponding solvatochromic shift in the absorbance maximum is less than 10 nm (Figure 6 e). We already showed that hydrogen bonding with water in tetrahydrofuran was accompanied by a similar spectral variation in the case of both di- and tetra-N-substituted oxoporphyrinogens.^[46] We ascribe the second and third sets of spectral

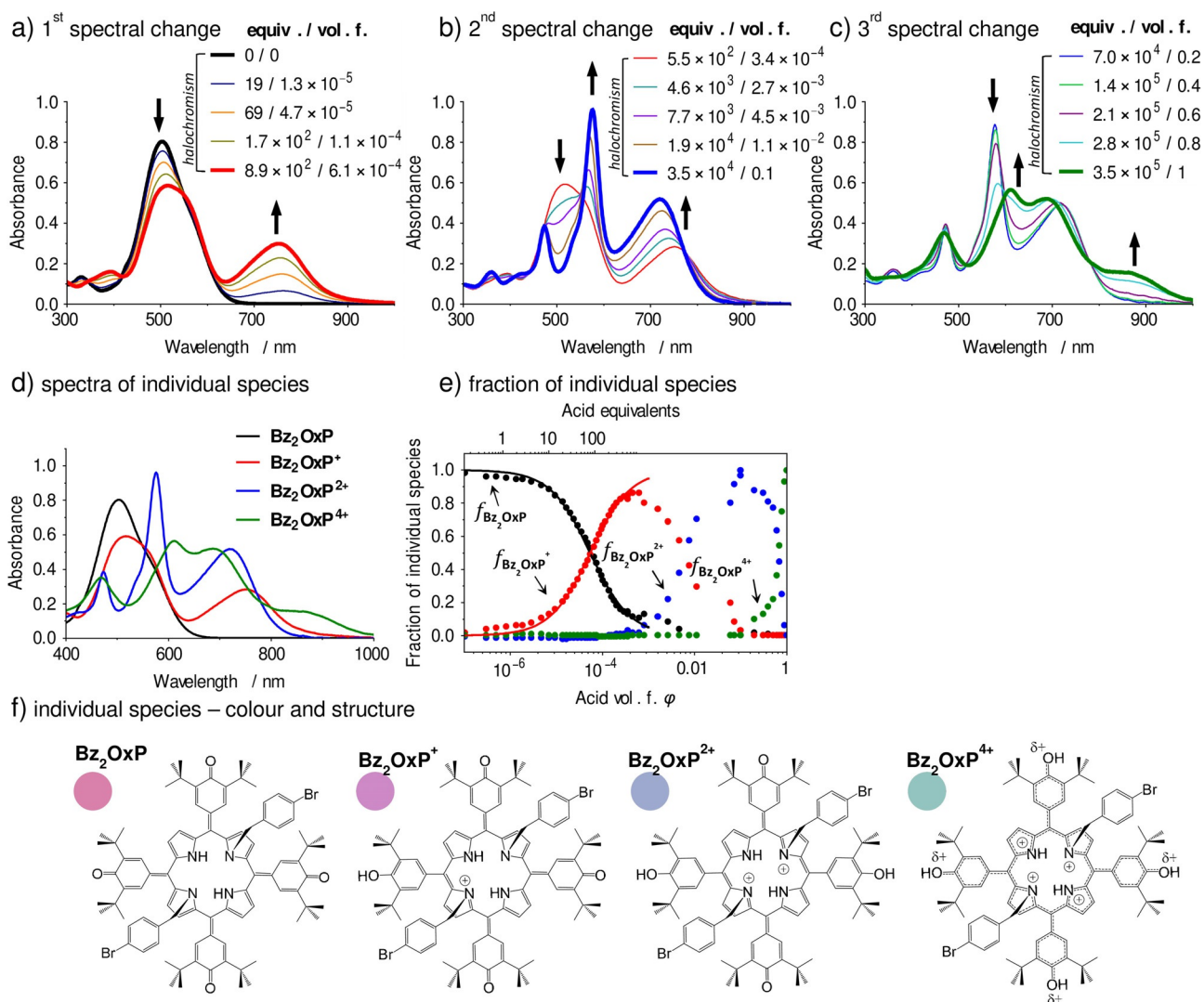


Figure 3. UV/Vis titration of Bz_2OxP (7×10^{-6} M in CDCl_3) with DFA. a–c) Three consecutive spectral changes occurring during titration. d) Spectra of individual absorbing species identified as start and endpoints of each spectral change (bold lines in panels a–c). e) Relative fraction of absorbing species obtained from SVD by fitting first spectral change with a 1:1 binding model (solid line); coefficients obtained by DSIS decomposition (solid circles). The same data in linear scale can be seen in Figure S14b. f) Chemical structures and colors of absorbing species (colors calculated from the spectra shown in panel d). The RGB coordinates are: Bz_2OxP (R=217, G=129, B=171), Bz_2OxP^+ (R=204, G=137, B=197), $\text{Bz}_2\text{OxP}^{2+}$ (R=157, G=169, B=206), and $\text{Bz}_2\text{OxP}^{4+}$ (R=147, G=196, B=192). Assignment of the chemical structures (including tautomeric processes) is given in Figure 11.

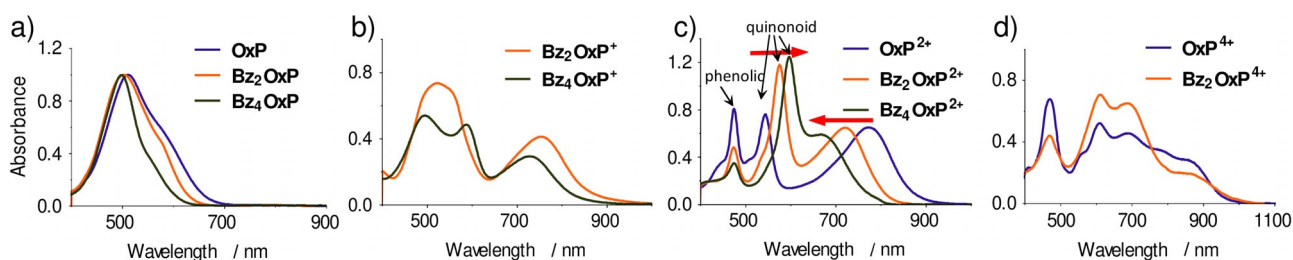


Figure 4. Spectra of neutral and protonated species of OxP , Bz_2OxP , and Bz_4OxP in the a) neutral state and in the b) monoprotated, c) diprotated, and d) tetraprotated forms. Spectra of neutral species were normalized to unity.

changes (Figure 6a,b) to protonation at the hemiquinonoid carbonyl atoms. We could again easily obtain spectra of mono- and diprotated species as pseudosaturation points during ti-

tration (Figure 6c). Assignments were made on the basis of comparisons with individual species of the other oxoporphyrinogens (Figure 4b,c). For vol. f. $\varphi > 0.01$ (i.e. halochromic be-

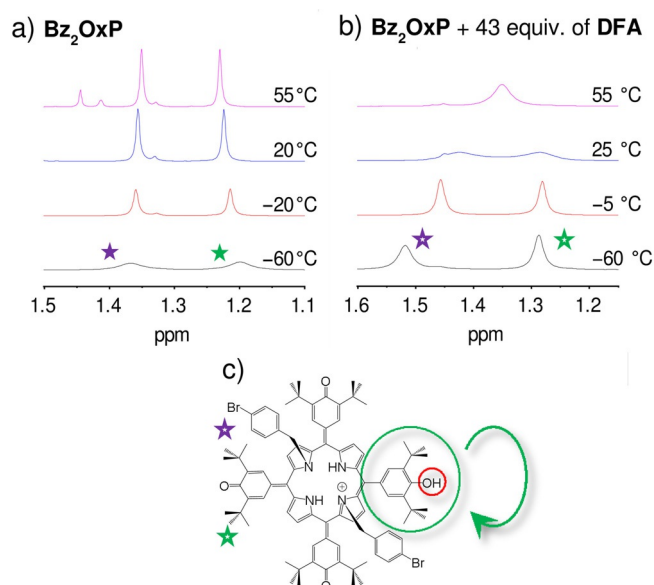


Figure 5. Demonstration of rotation of the **Bz₂OxP** hemiquinonoid groups due to increasing hydroxyphenyl character after protonation. a) There is no spectral change in the *tert*-butyl NMR signals upon varying the temperature in the absence of acid. b) Upon protonation, chemical exchange between both *tert*-butyl signals arises. c) The most plausible explanation is rotation of the whole *meso*-substituent group.

havior), we used a formula similar to that used in the previous cases for DSIS decomposition [Eq. (3)]:

$$S_{\text{obs}}(\varphi) = f_{\text{Bz}_4\text{OxP H-bond}}(\varphi) \times S_{\text{Bz}_4\text{OxP H-bond}} + f_{\text{Bz}_4\text{OxP}^+}(\varphi) \times S_{\text{Bz}_4\text{OxP}^+} + f_{\text{Bz}_4\text{OxP}^{2+}}(\varphi) \times S_{\text{Bz}_4\text{OxP}^{2+}} \quad (3)$$

Thus, for $\varphi > 0.01$, we obtained relative fractions of individual absorbing species (see Figure 6d). As in the previous cases, the quality of DSIS is excellent (Figure S6). SVD performed for $\varphi > 0.01$ confirmed the presence of three individual species in this concentration range (Figure S5). NMR titration of **Bz₄OxP** with DFA reveals a significant shift in the pyrrole β -proton resonance (Figure 7 and for chemical shifts as a function of acid volume fraction, see Figure S19c), which strongly suggests that positive charges are accommodated at the central nitrogen atoms of **Bz₄OxP** (Figure 6 f).

As shown in Figure 4, the spectra of the corresponding mono-, di-, and tetraprotonated species of each **OxP** derivative are similar in form, which we exploited to assign the degrees of protonation of each absorbing species. According to Table 1, **OxP** is easy to protonate twice and is stabilized by complexation through H-bonding of two counteranions at the central NH sites. Tetraprotonation is attained at about vol.f. $\varphi = 0.001$ of TFA. There exists strong positive cooperativity between the first and second protonation steps and between the third and fourth protonation steps (Table 1), so that spectra due to mono- and triprotonated states are not observable (similar to the case for double protonation of free-base porphyrins).^[43] **Bz₂OxP** can be easily monoprotated because of stabilization by one counteranion at the NH site. Full tetrapro-

tonation is not reached until the vol.f. of acid is close to 1. Similarly, the presence of strong cooperativity between the third and fourth protonations prevents direct observation of a triprotonated state during the UV/Vis titration experiment. Finally, **Bz₄OxP** is very difficult to protonate partly due to the lack of possible stabilization by counteranion binding and partly to steric crowding at the core of the molecule, which obstructs redistribution of the conjugation pathway for sharing of charge over electronegative heteroatoms (i.e. N and O, see Figure 1c). Complete protonation of **Bz₄OxP** is not possible even in neat acid. If we consider all the data relating to halochromism of these **OxP** derivatives, it is evident that N-alkylation makes protonation more difficult and concurrently shifts the range of colorimetric sensitivity to higher acid vol.f. To illustrate this potentially useful point, an overview of the color variation of these **OxP** derivatives is shown in Figure 8.

2.4. Mechanism of Halochromism

The **OxP** halochromic dye system is rather unique from the point of view of its mode of action. Most simple dye systems operate, whether solvatochromic or halochromic, on the basis of solvent polarity or protonation by mechanisms mentioned earlier, respectively. Conceptually, exceptions can be made on the basis of molecular design usually involving introduction of some complexing moiety to introduce specificity of analyte interaction to the dye.^[13,47] In this context, for **OxP**, halochromicity is strongly affected by the presence of the π -conjugated calix[4]pyrrole-type binding site, which introduces the possibility of counteranion binding and consequent stabilization of protonated species through ion-pair formation.

In the series **OxP**, **Bz₂OxP**, and **Bz₄OxP**, N-alkylation of the pyrrole groups effectively sequentially masks the binding site(s), disfavoring protonation by removing one source of stabilization (counteranion binding) and also by sterically restricting variation in the conjugated structure of the chromophore, which might otherwise stabilize protonated species. In fact, delocalization of charge in the **OxP** system may be one of the factors allowing the existence of the highly charged tetracation. In Figures 2e, 3 f, and 6 f, we have assigned the structures on the basis of formal placement of charge at the central nitrogen atoms. For lower degrees of protonation, these charges may be shared over all electronegative atoms, albeit with preference for the central nitrogen atoms. This feature is supported by NMR spectroscopy (Figures 9 and 10; for other acid titrations, see Figures S16–18), which shows that pyrrole proton resonances are strongly shifted downfield. The UV/Vis spectra offer further information about the state of the dyes under acidic conditions. For example, for **OxP**, double protonation results in red solutions due to tautomerization of the molecule to a porphodimethene form (Figure 11 a; also supported by NMR spectroscopy, see Figures 9 and S16), resulting in an apparent splitting of the broad **OxP** absorption band.^[48] This is due to the emergence of conjugated phenolic (at $\lambda = 465$ nm) and quinonoid (at $\lambda = 540$ nm) π - π^* absorptions (Figure 4c). These bands indicate the relative presence of these two types of moieties in the respective structures. For doubly protonated

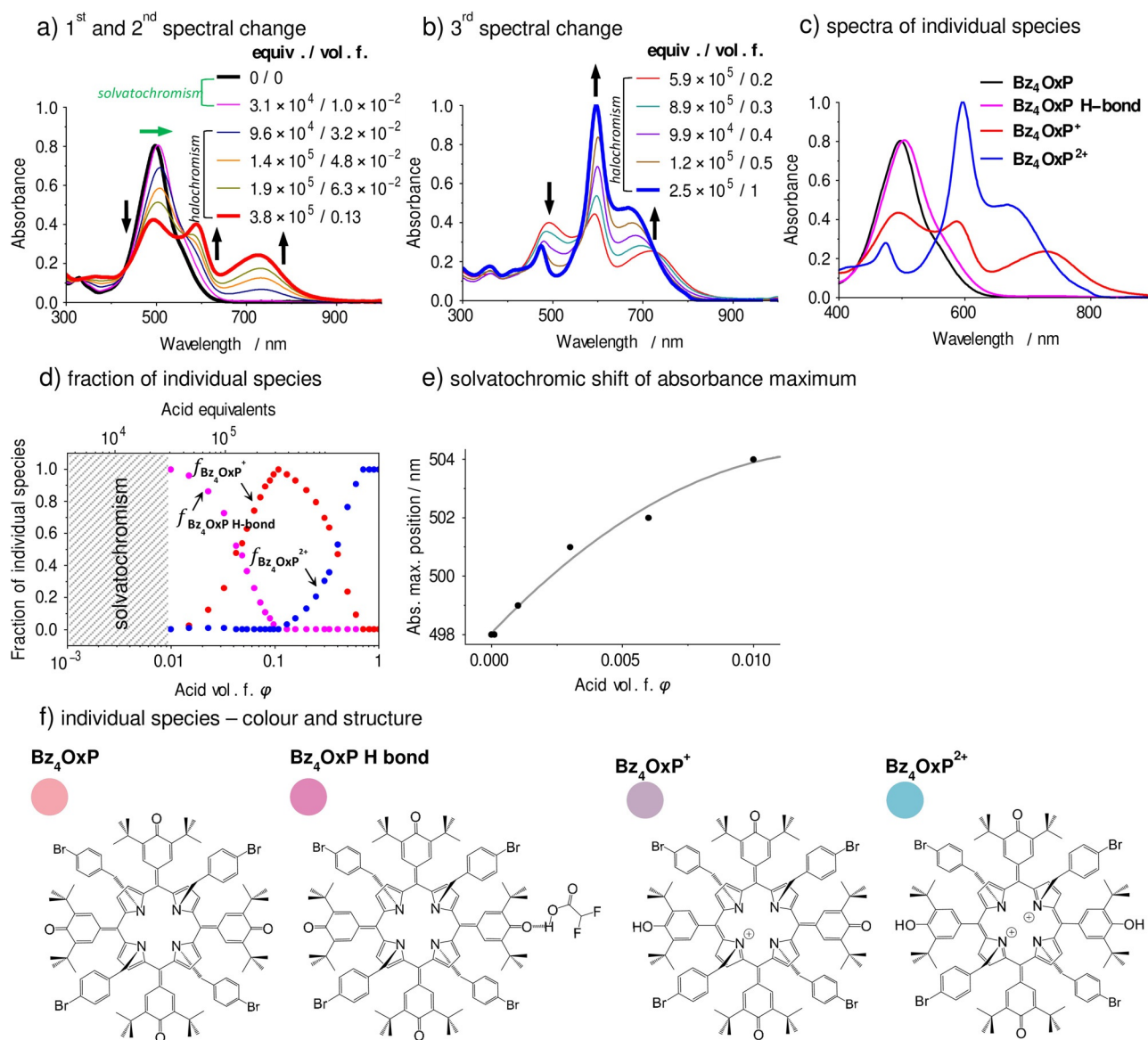


Figure 6. UV/Vis titration of Bz_4OxP (5×10^{-6} M in CDCl_3) with DFA. a, b) Three consecutive spectral changes occurring during titration. c) Spectra of individual absorbing species identified as start and endpoints of each spectral change (bold lines in panels a, b). d) Relative fraction coefficients obtained by DSIS. The same data in linear scale can be seen in Figure S14c. e) Solvatochromic shift of absorbance maxima for $\varphi < 0.01$ (hatched area in panel d). f) Chemical structures and colors of absorbing species (colors calculated from the spectra shown in panel c). The RGB coordinates are: Bz_4OxP (R = 244, G = 165, B = 173), Bz_4OxP H-bond (R = 225, G = 135, B = 184), Bz_4OxP^+ (R = 195, G = 168, B = 194), and $\text{Bz}_4\text{OxP}^{2+}$ (R = 121, G = 195, B = 213). Assignment of the chemical structures (including tautomeric processes) is given in Figure 11.

OxP, which has been forced to exist in its tautomeric form by protonation, the intensities of these bands correspond to the abundance of the phenol and quinonoid groups. Tetracationic species of **OxP** and Bz_2OxP are notable in that they have only weak contributions from the quinonoid band with prevalence of phenolic groups (Figure 4d). On the other hand, Bz_4OxP has only a very weak contribution of the $\lambda = 465$ nm band even in neat acid (Figure 4c). Thus, the effect of N-alkylation is two-fold: first it masks the binding site, which prevents counteranion binding; second, it effectively prevents reorganization of the chromophore through tautomerization even under conditions of high acidity. Examples of how delocalization might be depicted are shown for some of the compounds in Figure 11.

As shown in Figure 11 a, doubly protonated **OxP** gains stabilization through tautomerization (in addition to the stabilization it gains from anion-pair interactions). Figure 11 b shows how the positive charge introduced by protonation at the oxygen atom of Bz_2OxP is transmitted to a macrocycle nitrogen atom. Figure 11 c, d reveals that charge residing on the central nitrogen atoms can be effectively delocalized.

The broad, long wavelength band around $\lambda = 800$ nm in **OxP** is associated with guest binding at the pyrrole NH groups in **OxP** systems, and for example, it shifts sequentially to $\lambda = 740$ nm for Bz_2OxP and then to $\lambda = 690$ nm for Bz_4OxP (see Figure 4c) in their doubly protonated states. We assign this shift to reduction in conjugation due to the increasing non-co-

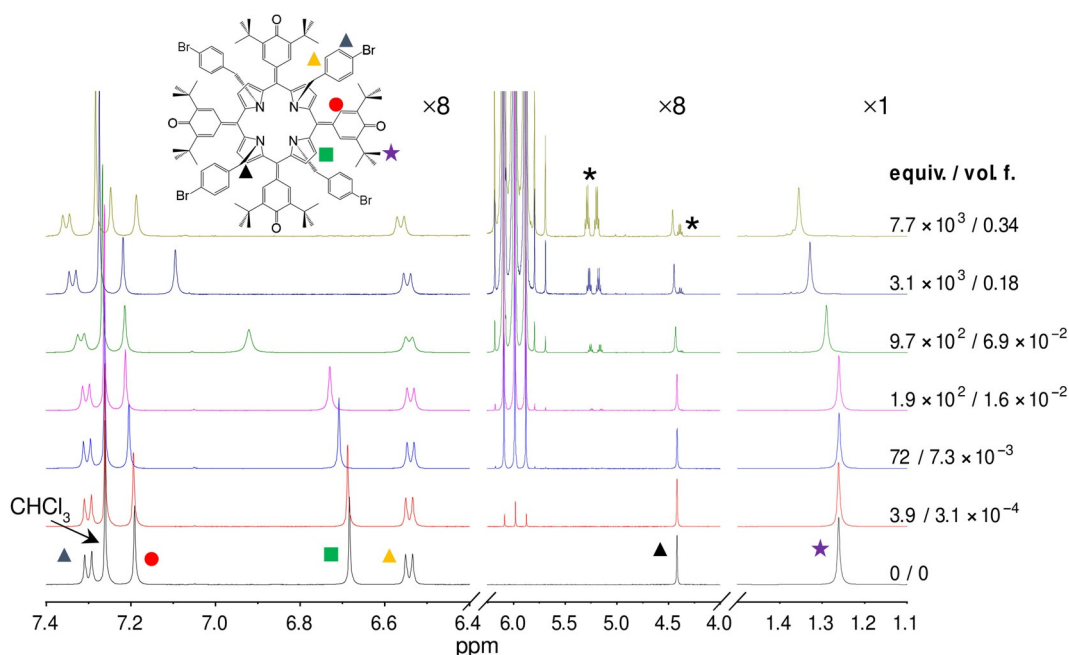


Figure 7. Titration of **Bz₄OxP** (8×10^{-4} M in CDCl_3) with DFA. Asterisk (*) denotes impurities contained in acid. Some regions of the spectra are magnified for clarity. The factor of magnification is given above each region. See Figure S19 for the chemical shifts of the respective resonances during the titration.

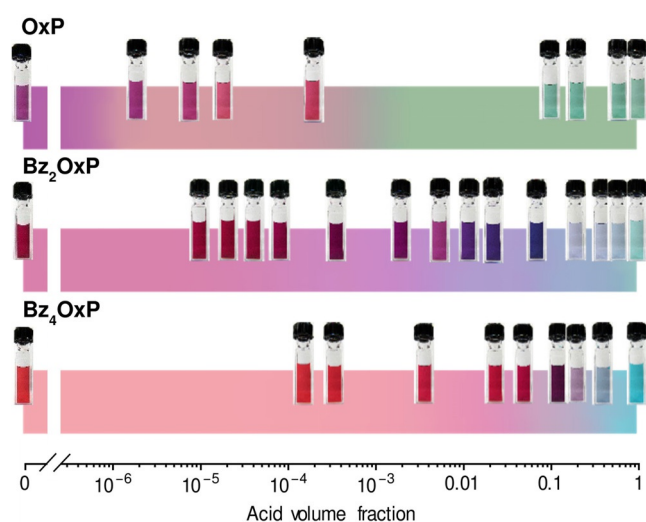


Figure 8. Colorimetric response of **OxP** (with TFA), **Bz₂OxP**, and **Bz₄OxP** (with DFA) over the entire concentration range of the acids. Colors shown were obtained by interpolation from the actual measured spectra (Figures 2, 3, and 6), and the scales are overlaid with photographs of the sample cuvettes (from the titration experiments) at the appropriate vol.f.

planarity of the moieties caused by increasing steric hindrance at the macrocyclic core.

Some of the changes caused by protonation (i.e. halochromism) in the **OxP** series bear analogy with the solvatochromic merocyanine dyes (e.g. Brooker's merocyanine),^[4,5,49,50] for which electron density is distributed over electronegative atoms depending on the prevailing polarity, with zwitterionic and neutral states being stabilized in polar and nonpolar solvents, respectively. For **OxP**, initial protonation at the carbonyl oxygen atoms leads to a tautomerization-like process, for

which positive charge is relocated and accommodated largely at the macrocyclic nitrogen atoms. Pyrrole nitrogen atoms cannot be directly protonated unless **OxP** is in its tautomerized porphodimethene form, which contains imino nitrogen atoms (this form can be stabilized by interactions with a polar solvent, see Figure 13a and discussion below). In contrast, tautomerization in **Bz₂OxP** and **Bz₄OxP** is precluded by N-alkyl groups, so that initial protonation must occur at the carbonyl oxygen atom. Protonation-induced tautomerization in **OxP** is now a relatively well-understood phenomenon. However, solvent-polarity-induced tautomerization of **OxP** is not a well-studied feature.

2.5. Solvatochromic Effects

To examine any solvatochromic properties of the **OxP** derivatives, we investigated their behavior in dimethylformamide (DMF)/chloroform binary mixtures (Figure 12). All three compounds show solvatochromism (similar to the first spectral change for the **Bz₄OxP**–DFA interaction, Figure 6a) manifested as a bathochromic shift, as shown in Figure 12a,e,g (green arrow). The central NH binding sites of **OxP** and **Bz₂OxP** enable interaction with DMF, resulting in other spectral changes (two changes for **OxP** and one change for **Bz₂OxP**), see Figure 12b,c,e. Hydrogen bonding between **OxP** derivatives and solvents including water and carbonyl-containing solvents (e.g. acetone)^[34] is known and can be described for **OxP** and **Bz₂OxP**, as shown in Figure 13. For **OxP** (Figure 12a), at low vol.f. of DMF, the bathochromic shift is followed at higher vol.f. DMF by a second spectral change, which we associate with a tautomeric process similar to that occurring during its protonation (according to a comparison of Figure 12b red line with Figure 2a blue line). As **OxP** undergoes further spectral

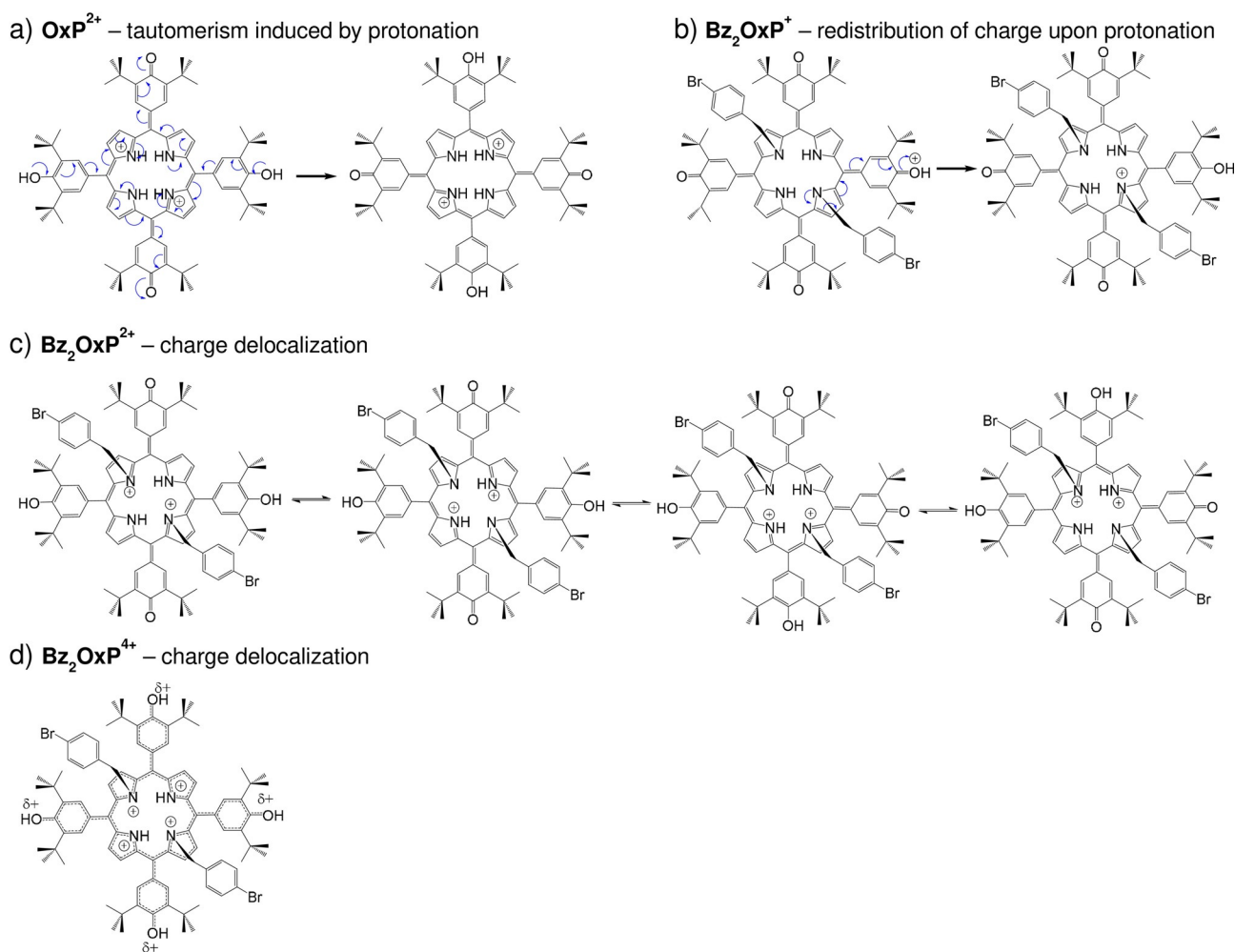


Figure 11. Redistribution of charge upon protonation for a) OxP and b–d) Bz_2OxP .

(form 2), is only stable around 1.4×10^{-2} vol.f. of DMF]. The proposed individual absorbing species of OxP are shown in Figure 13a. Interestingly, the tautomer form of OxP can only accommodate a single DMF guest through H-bonding at the macrocycle, as the tautomer also possesses imino-type nitrogen atoms that cannot bind DMF. Phenol groups in the tautomer may H-bond with DMF, although this interaction ought to be weakened by steric effects of the *tert*-butyl groups. At increasing DMF vol.f., the calix[4]pyrrole form is preferred, as binding of two DMF guests stabilizes that form. For Bz_2OxP , despite some variation in its UV/Vis spectrum during titration with DMF (Figure 12e), it does not undergo any tautomeric processes denoted by the lack of the absorbance maximum at $\lambda = 465$ nm (Figure 4c). We assign the second spectral change (Figure 12e, red line) to binding of DMF at the macrocyclic core (see Figure 13b, form 2). Similarly, there are no further spectral changes for Bz_4OxP from the point of view of tautomerism (Figure 12g). The solvatochromic shift of the spectral maximum of Bz_4OxP is shown in Figure S14f.

As in the case of protonation, we were able to isolate spectra of individual absorbing species as endpoints of spectral variations (Figure 12d,f,h). Although pure solvatochromic

changes cannot, in principle, be decomposed by using DSIS (as mentioned before for Reichardt's dye), other spectral changes (tautomeric and binding processes of OxP and Bz_2OxP) can be analyzed by this method (Figures S7–S10 and Figure S14d,e in linear scale). An overview of the color variation of the OxP derivatives for the whole DMF concentration range can be seen in Figure 14.

3. Conclusions

In summary, we present tetrakis(3,5-di-*tert*-butyl-4-oxocyclohexadien-2,5-yl)porphyrinogen (OxP) and its $\text{N}_{21},\text{N}_{23}$ -bis(4-bromobenzyl) and $\text{N}_{21},\text{N}_{22},\text{N}_{23},\text{N}_{24}$ -tetrakis(4-bromobenzyl) derivatives (Bz_2OxP and Bz_4OxP , respectively) as a series of halochromic dyes that operate as colorimetric indicators over a very broad range of acid contents in nonpolar media. This was permitted by up to fourfold protonation of the OxP derivatives. The maximum protonation level was tuned by N-alkylation, which effectively shifted the sensitivity (colorimetric range) to higher acid contents, as protonation of the molecules was increasingly obstructed. This was manifested as a gradual change in color over a broad range of acid contents (from volume frac-

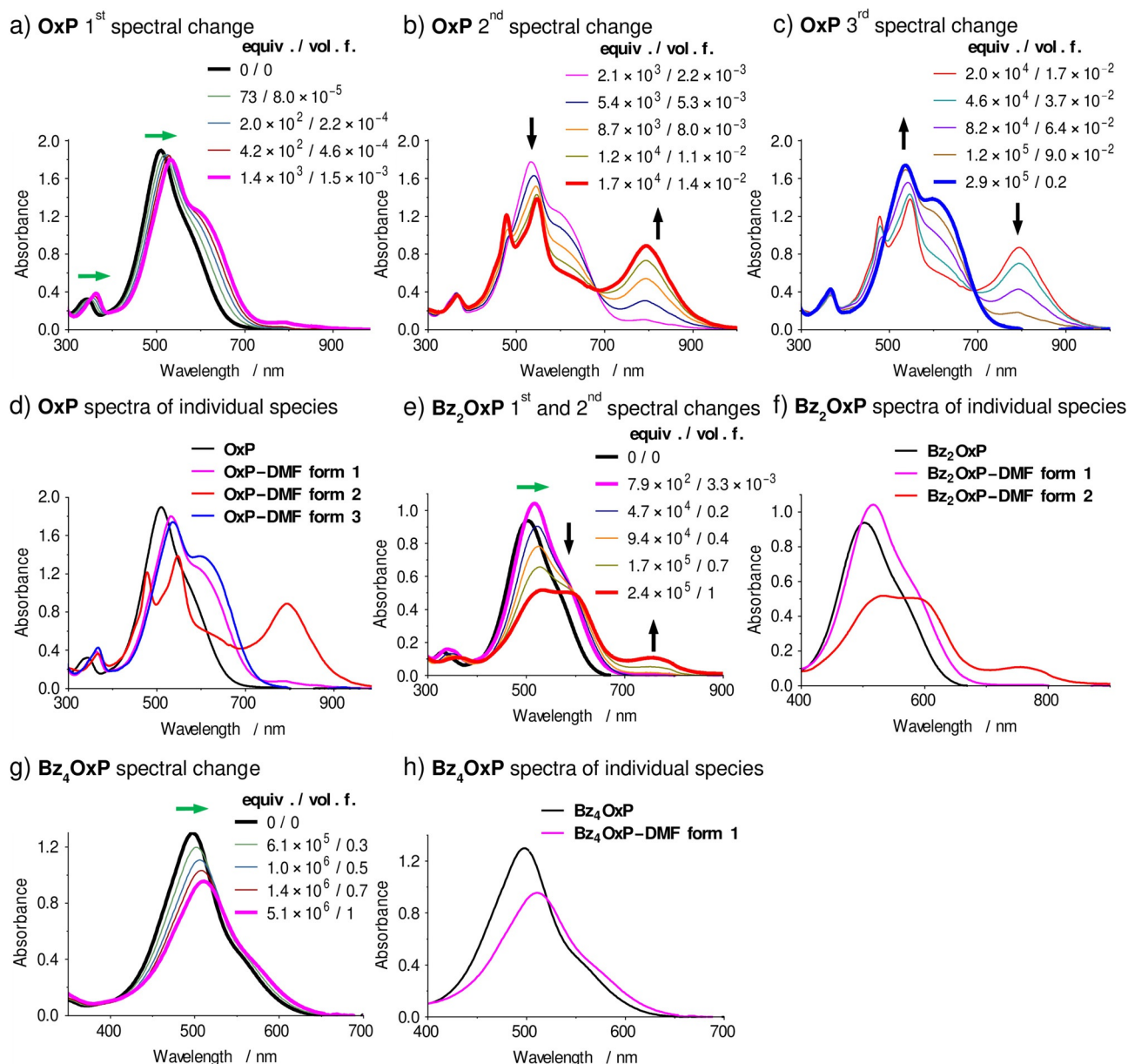


Figure 12. Solvatochromism of the investigated OxP derivatives in a binary mixture of chloroform/DMF; spectra taken from zero DMF concentration up to saturation. a–c) DMF-concentration-dependent consecutive spectral changes of OxP. d) Isolated spectra of individual species from the starting and endpoint spectra, as obtained from panels a–c. e) Spectral changes of Bz₂OxP and f) corresponding isolated individual absorption spectra. g) Spectral change of Bz₄OxP and h) corresponding isolated individual absorption spectra.

tions of 10^{-7} to nearly 1) over the series OxP, Bz₂OxP, and then Bz₄OxP. The mechanism of operation involves stabilization by counteranion binding, which enables colorimetric detection of small amounts of acid (less than 10^{-6} M). For Bz₄OxP, stabilization by a counteranion was not permitted, so that its response was limited to higher acid contents (from volume fractions of 0.1). Our analysis was supported by UV/Vis spectrophotometric measurements, for which the spectra of the individual components were isolated, and also by NMR spectroscopy.

In the case of the series OxP, Bz₂OxP, and Bz₄OxP, our molecular design concept was initially based on binding-site blocking and its effect on colorimetric response. It was predicted that the lack of binding sites would lead to a gradual nega-

tion of any colorimetric response. However, in the case of acids, we were surprised to discover the retention of response to acid analytes, even in the completely blocked derivative Bz₄OxP. A further advantage of this OxP-based indicator system is that the compounds have similar structures and properties, perhaps facilitating their application as blends of OxP derivatives and avoiding any mismatches in, for example, their solubilities. We believe that the concurrent effects of binding-site blocking and modulation of acidity sensitivity are important new aspects for the development of colorimetric indicators for various applications.

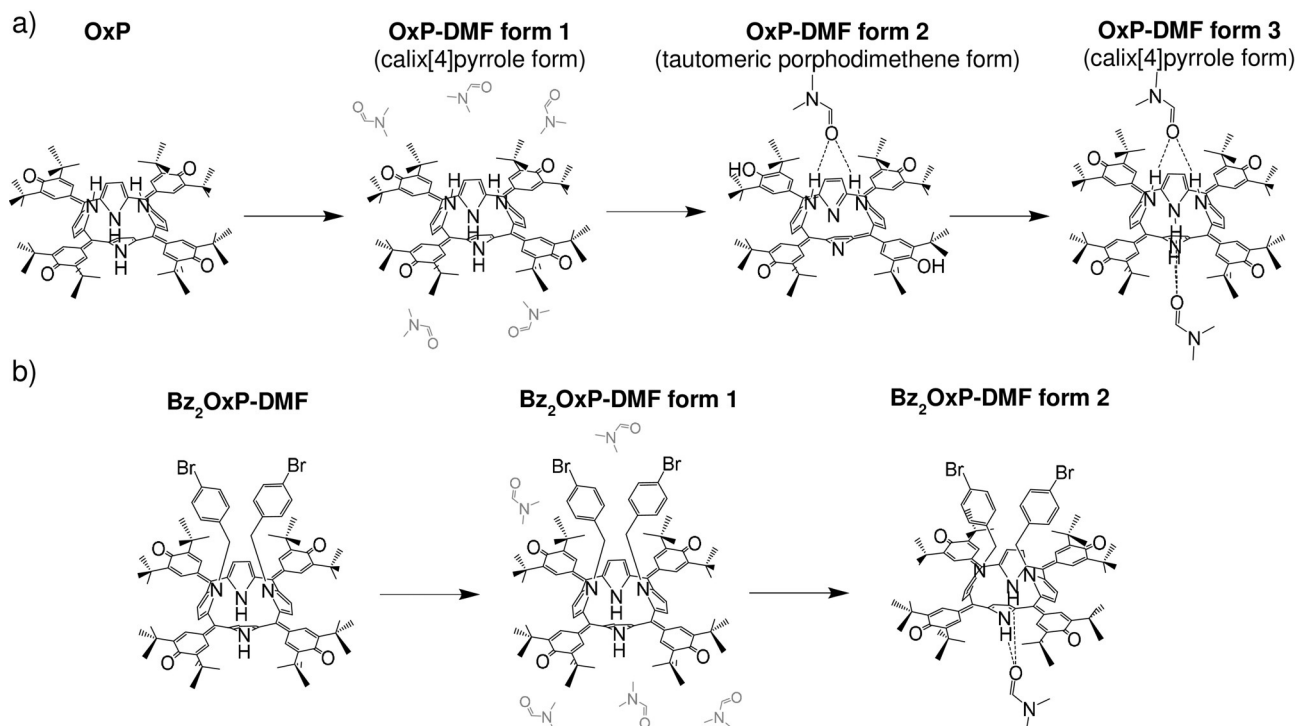


Figure 13. Suggested structures of individual species of oxoporphyrinogens in chloroform/DMF solution: a) OxP and b) Bz₂OxP.

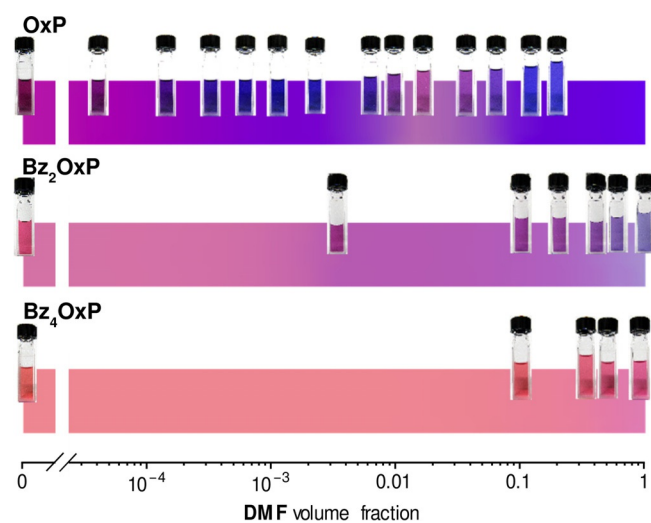


Figure 14. Colorimetric response of OxP derivatives over the entire concentration range of DMF. Colors shown were obtained by interpolation from the actual measured spectra (Figure 12), and the scales are overlaid with photographs of sample cuvettes (from the titration experiments) at the appropriate vol. f.

Experimental Section

Chemicals

OxP and its derivatives were prepared by a previously reported method.^[29,51,52] We used silver-foil-stabilized deuterated chloroform (CDCl₃) as the solvent and camphorsulfonic acid in powder form and liquid difluoroacetic acid as reagents (Sigma-Aldrich). Difluoroacetic acid (DFA) was chosen instead of commonly used trifluoroacetic acid (TFA) due to the presence of a nonexchanging proton

and its associated ¹H NMR signal. Samples containing oxoporphyrinogen derivatives and excess amounts of DFA were stored in the dark to avoid photoinduced chemical changes.

Camphorsulfonic acid (CSA) is poorly soluble in chloroform (≈0.02 M). Difluoroacetic acid and chloroform (in the presence of the OxP derivative) are miscible for arbitrary volume fractions.

Instrumentation

UV/Vis absorption spectra were recorded by using Jasco J-820, Shimadzu UV-3600, and Hitachi U-2910 spectrophotometers (1 cm or 1 mm quartz cells with screw caps were used). NMR spectroscopy was performed by using Bruker Avance III HD 500 and JEOL AL300BX spectrometers. Tetramethylsilane was used as the internal standard. Titration experiments were performed by the addition of stock solution (acid dissolved in chloroform) into the sample by using a microsyringe. All measurements were performed at 25 °C unless otherwise specified.

Data-Processing methods

The conversion of the measured UV/Vis spectra into the corresponding RGB values was conducted by using the Spectral calculator.^[53] Processing of UV/Vis data by using singular value decomposition (SVD) and decomposition into the spectra of individual species (DSIS) were performed according to the technical details given in the Supporting Information. Also, binding models (isotherms) used for UV/Vis and NMR spectroscopy data are discussed in detail in the Supporting information.

Acknowledgements

The study was partially supported by the Grant Agency of Charles University (project GA UK, No. 718214), Japan Society for the Promotion of Science (JSPS) KAKENHI Grant No. JP15K13684, JSPS KAKENHI Grant No. JP16H06518 (Coordination asymmetry), and Core Research for Evolutional Science and Technology (CREST), Japan Science and Technology Agency (JST), Japan (Grant No. JPMJCR1665). This work was also partly supported by World Premier International Research Center Initiative (WPI Initiative), Ministry of Education, Culture, Sports, Science and Technology (MEXT), Japan. The Bruker NMR spectrometer was purchased within the project CZ.2.16/3.1.00/21566 funded by the Operational Programme Prague-Competitiveness.

Conflict of Interest

The authors declare no conflict of interest.

Keywords: calixpyrroles · halochromism · NMR spectroscopy · solvatochromism · UV/Vis spectroscopy

- [1] K. Yamaguchi, T. Murai, J.-D. Guo, T. Sasamori, N. Tokitoh, *ChemistryOpen* **2016**, *5*, 434–438.
- [2] A. S. Choudhary, S. R. Patil, N. Sekar, *Color. Technol.* **2016**, *132*, 387–398.
- [3] C. Reichardt, *Chem. Rev.* **1994**, *94*, 2319–2358.
- [4] E. M. Kosower, *J. Am. Chem. Soc.* **1958**, *80*, 3253–3260.
- [5] E. M. Kosower, *J. Am. Chem. Soc.* **1958**, *80*, 3261–3267.
- [6] *Photochromism: Molecules and Systems* (Eds.: H. Dürr, H. Bouas-Laurent), Elsevier, Amsterdam, **2003**.
- [7] M. Okamoto, S. Hirayama, R. P. Steer, *Can. J. Chem.* **2007**, *85*, 432–437.
- [8] *Organic Photochromic and Thermochromic Compounds: Vol 2: Physicochemical Studies, Biological Applications, and Thermochromism* (Eds.: J. C. Crano, R. J. Guglielmetti), Kluwer Academic Publishers, New York, **2002**.
- [9] A. Shundo, S. Ishihara, J. Labuta, Y. Onuma, H. Sakai, M. Abe, K. Ariga, J. P. Hill, *Chem. Commun.* **2013**, *49*, 6870–6872.
- [10] F. G. Bordwell, *Acc. Chem. Res.* **1988**, *21*, 456–463.
- [11] I. Leito, T. Rodima, I. A. Koppel, R. Schwesinger, V. M. Vlasov, *J. Org. Chem.* **1997**, *62*, 8479–8483.
- [12] A. Baeyer, V. Villiger, *Ber. Dtsch. Chem. Ges.* **1902**, *35*, 1189–1201.
- [13] C. Reichardt, *Chem. Soc. Rev.* **1992**, *21*, 147–153.
- [14] L. S. Foster, I. J. Grunfest, *J. Chem. Educ.* **1937**, *14*, 274–276.
- [15] L. M. Zimmermann-Dimer, V. G. Machado, *Dyes Pigment.* **2009**, *82*, 187–195.
- [16] L. R. Milgrom, *The Colors of Life: An Introduction to the Chemistry of Porphyrins and Related Compounds*, Oxford University Press, Oxford, **1997**.
- [17] A. Stone, E. B. Fleischer, *J. Am. Chem. Soc.* **1968**, *90*, 2735–2748.
- [18] B. M. Harvey, P. E. Hoggard, *Monatsh. Chem.* **2012**, *143*, 1101–1105.
- [19] F. Hibbert, K. P. P. Hunte, *J. Chem. Soc. Perkin Trans. 2* **1977**, *12*, 1624–1628.
- [20] L. Guo, *J. Colloid Interface Sci.* **2008**, *322*, 281–286.
- [21] S. M. Andrade, R. Teixeira, S. M. B. Costa, A. J. F. N. Sobral, *Biophys. Chem.* **2008**, *133*, 1–10.
- [22] *The Porphyrin Handbook Vol. 1–9* (Eds.: K. M. Kadish, K. M. Smith, R. Guilard), Academic Press, San Diego, CA, **2000**.
- [23] For example: A. K. Mandal, M. Taniguchi, J. D. Diers, D. M. Niedzwiedzki, C. Kirmaier, J. S. Lindsey, D. F. Bocian, D. Holten, *J. Phys. Chem. A* **2016**, *120*, 9719–9731.
- [24] *The Porphyrin Handbook Vol. 3: Inorganic, Organometallic and Coordination Chemistry* (Eds.: K. M. Kadish, K. M. Smith, R. Guilard), Academic Press, San Diego, CA, **2000**.
- [25] For example: N. Chaudhri, M. Sankar, *RSC Adv.* **2015**, *5*, 3269–3275.
- [26] H. Furuta, T. Asano, T. Ogawa, *J. Am. Chem. Soc.* **1994**, *116*, 767–768.
- [27] H. Furuta, H. Maeda, A. Osuka, *J. Am. Chem. Soc.* **2000**, *122*, 803–807.
- [28] For example: J. Aimi, Y. Nagamine, A. Tsuda, A. Muranaka, M. Uchiyama, T. Aida, *Angew. Chem. Int. Ed.* **2008**, *47*, 5153–5156; *Angew. Chem.* **2008**, *120*, 5231–5234.
- [29] J. L. Sessler, P. A. Gale in *The Porphyrin Handbook Vol. 6: Applications: Past, Present, and Future* (Eds. K. M. Kadish, K. M. Smith, R. Guilard), Academic Press, San Diego, CA, **2000**, pp. 257–278.
- [30] J. L. Sessler, P. Anzenbacher, Jr., K. Jursikova, H. Miyaji, J. W. Genge, N. A. Tvermoes, W. E. Allen, J. A. Shriver, P. A. Gale, V. Kral, *Pure Appl. Chem.* **1998**, *70*, 2401–2408.
- [31] P. A. Gale, J. L. Sessler, V. Kral, *Chem. Commun.* **1998**, *1*, 1–8.
- [32] S. K. Kim, J. L. Sessler, *Acc. Chem. Res.* **2014**, *47*, 2525–2536.
- [33] J. P. Hill, A. L. Schumacher, F. D'Souza, J. Labuta, C. Redshaw, M. R. J. Elsegood, M. Aoyagi, T. Nakanishi, K. Ariga, *Inorg. Chem.* **2006**, *45*, 8288–8296.
- [34] L. R. Milgrom, J. P. Hill, G. Yahioglu, *J. Heterocycl. Chem.* **1995**, *32*, 97–101.
- [35] E. Dolušić, S. Toppet, S. Smeets, L. V. Meervelt, B. Tinant, W. Dehaen, *Tetrahedron* **2003**, *59*, 395–400.
- [36] F. D'Souza, N. K. Subbaiyan, Y. Xie, J. P. Hill, K. Ariga, K. Ohkubo, S. Fukuzumi, *J. Am. Chem. Soc.* **2009**, *131*, 16138–16146.
- [37] J. P. Hill, I. J. Hewitt, C. E. Anson, A. K. Powell, A. L. McCarthy, P. A. Karr, M. E. Zandler, F. D'Souza, *J. Org. Chem.* **2004**, *69*, 5861–5869.
- [38] E. R. Henry, J. Hofrichter in *Methods in Enzymology Vol. 210: Numerical Computer Methods* (Eds.: L. Brand, M. L. Johnson), Academic Press, San Diego, CA, **1992**, pp. 129–192.
- [39] E. R. Malinowski, *Factor Analysis in Chemistry*, Wiley, New York, **2002**.
- [40] P. Mojzeš, P. Praus, V. Baumruk, P.-Y. Turpin, P. Matoušek, M. Towrie, *Biopolymers* **2002**, *67*, 278–281.
- [41] J. Palacký, P. Mojzeš, J. Bok, *J. Raman Spectrosc.* **2011**, *42*, 1528–1539.
- [42] J. Labuta, Z. Futera, S. Ishihara, H. Kouřilová, Y. Tateyama, K. Ariga, J. P. Hill, *J. Am. Chem. Soc.* **2014**, *136*, 2112–2118.
- [43] J. Labuta, S. Ishihara, A. Shundo, S. Arai, S. Takeoka, K. Ariga, J. P. Hill, *Chem. Eur. J.* **2011**, *17*, 3558–3561.
- [44] C. J. Medforth, P. E. Berget, J. C. Fetting, K. M. Smith, J. A. Shelnett, *J. Porphyrins Phthalocyanines* **2016**, *20*, 307–317.
- [45] S. Thyagarajan, T. Leiding, S. P. Arskold, A. V. Cheprakov, S. A. Vinogradov, *Inorg. Chem.* **2010**, *49*, 9909–9920.
- [46] S. Ishihara, J. Labuta, T. Šikorský, J. V. Burda, N. Okamoto, H. Abe, K. Ariga, J. P. Hill, *Chem. Commun.* **2012**, *48*, 3933–3935.
- [47] V. G. Machado, R. I. Stock, C. Reichardt, *Chem. Rev.* **2014**, *114*, 10429–10475.
- [48] This spectral change was initially assigned to symmetry breaking of the tetrapyrrole core with a resulting split in the Soret band similar to the differences observed in the visible region of electronic absorption spectra of free-base porphyrins relative to simple metalloporphyrins.^[9]
- [49] V. Z. Shirinian, A. A. Shimkin, *Top. Heterocycl. Chem.* **2008**, *14*, 75–105.
- [50] J. O. Morley, R. M. Morley, R. Docherty, M. H. Charlton, *J. Am. Chem. Soc.* **1997**, *119*, 10192–10202.
- [51] L. R. Milgrom, *Tetrahedron* **1983**, *39*, 3895–3898.
- [52] J. P. Hill, W. Schmitt, A. L. McCarty, K. Ariga, F. D'Souza, *Eur. J. Org. Chem.* **2005**, *2005*, 2893–2902.
- [53] B. Lindbloom, spectral calculator, <http://www.bruceindbloom.com/> (accessed on March 9, 2018).

Received: January 9, 2018

Version of record online April 20, 2018